Green Energy and Resources 4 (2026) 100200

Contents lists available at ScienceDirect

Green Energy and Resources

journal homepage: www.journals.elsevier.com/green-energy-and-resources

Research Article

Improving the efficiency of CO_2 utilization in vertical farming via CFD modelling with consideration of leaf microstructure

Shengchun Liu[a], Chenxing Wang[a], Lanfang Hu[a], Luna Guo[a,*], Xiaolin Wang[b], Anders Avelin[b], Hailong Li[b,*]

[a] Key Laboratory of Refrigeration Technology of Tianjin, Tianjin University of Commerce, Tianjin, 300134, China
[b] School of Business, Society and Technology, Mälardalen University, Västerås, 72123, Sweden

ARTICLE INFO

Keywords:
Vertical farming (VF)
Photosynthesis
Carbon dioxide enrichment
Plant model
Computational Fluid dynamics (CFD)
Leaf microstructure

ABSTRACT

Vertical farming (VF), as a promising solution to mitigating multifaceted challenges posed by global population growth and urbanization, needs supplementing carbon dioxide (CO_2), an essential substrate for photosynthesis, to promote plant growth. Optimizing the CO_2 supply to reduce operational costs relies on accurate modelling of CO_2 distribution and intake within VF chambers. For such an objective, this research constructed an innovative computational fluid dynamics (CFD) model that can explicitly incorporate the effects of leaf microstructure on CO_2 absorption to simulate CO_2 interactions between plants and environment more accurately. After validation, the model was employed to investigate CO_2 distribution, photosynthetic rate, and total CO_2 consumption, using wheat as a studied crop due to data availability. Compared to previous models that ignore CO_2 diffusion within leaves, the new model shows a decrease in the daily CO_2 uptake by 8.1%, and consequently the consumption of pure CO_2 is reduced by 8.5%. Such findings reveal that incorporating the leaf microstructure is important to improve the accuracy in modelling CO_2 supplementation and avoid the overestimation of CO_2 utilization efficiency.

Nomenclature

A	photosynthesis rate (μmol CO_2 $m^{-2}{\cdot}s^{-1}$)	O_2	O_2 partial pressure (mbar)
A_G	gross photosynthesis rate (μmol CO_2 $m^{-2}{\cdot}s^{-1}$)	P	power (W)
A^*_G	overall volumetric photosynthesis rate of chloroplasts (μmol CO_2 $m^{-3}{\cdot}s^{-1}$)	P_m	CO_2 permeability through the cell membrane ($m{\cdot}s^{-1}$)
B	net $CO_2 \rightarrow HCO_3^-$ hydration rate ($mol{\cdot}m^{-3}{\cdot}s^{-1}$)	R	Reynolds
C_a	atmospheric CO_2 levels ($\mu mol{\cdot}mol^{-1}$)	R_d	day respiration (μmol CO_2 $m^{-2}{\cdot}s^{-1}$)
C_c	mesophyll CO_2 concentration ($\mu mol{\cdot}mol^{-1}$)	R^*_d	volumetric respiration rate (μmol CO_2 $m^{-3}{\cdot}s^{-1}$)
$C_{HCO3^-,c}$	HCO_3^- concentration in chloroplasts ($mol{\cdot}m^{-3}$)	Re	Reynolds number
C_i	intercellular CO_2 concentration ($\mu mol{\cdot}mol^{-1}$)	S	Schmidt number of turbulence
C_j	the CO_2 concentration in phase j	S_m	user-defined source term ($kg{\cdot}m^{-3}{\cdot}s^{-1}$)
		S_T	heat source or sink ($W{\cdot}m^{-3}$)

(*continued on next column*)

(*continued*)

C_F	Nonlinear momentum loss coefficient	s	slope coefficient for transforming Photosystem II (PSII) electron transport efficiency derived from chlorophyll fluorescence to J (−)
C_p	specific heat ($J{\cdot}kg^{-1}{\cdot}K^{-1}$)	T	room temperature (K)
D	drag coefficient	T_{leaf}	leaf temperature (K)
D_j	diffusivity of phase j ($m^2{\cdot}s^{-1}$)	T_p	chloroplast export rate of the triose phosphate ($\mu mol{\cdot}m^{-2}{\cdot}s^{-1}$)
D_c	diffusivity of CO_2 in	τ	time (s)
D_{epi}	mesophyll cytoplasm ($m^2{\cdot}s^{-1}$), epidermis layer	u	velocity vector component ($m{\cdot}s^{-1}$)
D_w	($m^2{\cdot}s^{-1}$), and cell wall ($m^2{\cdot}s^{-1}$)	V	volume of growing area (m^3)
$D_{HCO3^-,c}$	HCO_3^- diffusion rate within the mesophyll cell cytoplasm ($m^2{\cdot}s^{-1}$)	$V_{c,max}$	Maximum rate of Ribulose-1,5-bisphosphate carboxylase/oxygenase (Rubisco) activity-limited carboxylation ($\mu mol{\cdot}m^{-2}{\cdot}s^{-1}$)
d	mean tissue thickness (m)	ν	diffusion velocity ($m{\cdot}s^{-1}$)

(*continued on next page*)

* Corresponding authors.
E-mail addresses: guoluna@tjcu.edu.cn (L. Guo), hailong.li@mdu.se (H. Li).

https://doi.org/10.1016/j.gerr.2026.100200
Received 12 January 2026; Received in revised form 25 May 2026; Accepted 31 May 2026
2949-7205/© 2026 The Authors. Published by Elsevier B.V. on behalf of Shandong University. This is an open access article under the CC BY license (http://creativecommons.org/licenses/by/4.0/).

(*continued*)

E	total consumption of CO_2 (μmol)	w_c	rate of Rubisco activity-limited carboxylation ($\mu mol \cdot m^{-2} \cdot s^{-1}$)
f_c	the fraction of chloroplasts of the leaf	w_j	electron transport-limited carboxylation rate ($\mu mol \cdot m^{-2} \cdot s^{-1}$)
f_m	the fraction of cytosols of the leaf	w_p	rate of triose phosphate utilization (TPU) limited carboxylation ($\mu mol \cdot m^{-2} \cdot s^{-1}$)
g	gravitational acceleration ($m \cdot s^{-2}$)	Y_i	mass fraction of substance i ($kg \cdot m^{-3}$)
H	CO_2 Henry's constant ($mol \cdot m^{-3}$ liquid) ($mol \cdot m^{-3}$ gas)$^{-1}$	*Greek letters*	
$[H^+]$	H^+ concentration ($mol \cdot L^{-1}$)	ϕ	CO_2 flux through the membrane ($\mu mol \cdot m^{-2} \cdot s^{-1}$)
I_{inc}	photon flux density reaching leaves (μmol photon $m^{-2} \cdot s^{-1}$)	Γ^*	CO_2 compensation point based on C_c without R_d ($\mu mol \cdot mol^{-1}$ or μbar)
J	the chlorophyll fluorescence-derived electron transport rate (μmol electron $m^{-2} \cdot s^{-1}$)	λ	thermal conductivity ($W \cdot m^{-1} \cdot K^{-1}$)
J_i	mass diffusion flux of substance i	μ	dynamic viscosity ($kg \cdot m^{-1} \cdot s^{-1}$)
k_1	CO_2 hydration and	ρ	fluid density ($kg \cdot m^{-3}$)
k_2	dehydration velocity constant (s^{-1})	*Terms and abbreviations*	
K	acidity constant of carbonic acid ($mol \cdot L^{-1}$)	CFD	computational fluid dynamics
$K_{m,C}$	Rubisco's Michaelis constant	*LAD*	leaf area density ($m^2 \cdot m^{-3}$)
$K_{m,O2}$	for CO_2 ($\mu mol \cdot mol^{-1}$ or μbar) and O_2 (mbar)	LED	light-emitting diodes
K_p	permeability of porous medium (m^2)	UDF	user-defined functions
Nu	Nusselt number	VF	vertical farm

1. Introduction

Vertical farming (VF) is emerging as an innovative solution to address the challenges of increasing global demand for food and sustainable development in rapidly urbanising areas (Dsouza et al., 2023; Vasavi et al., 2025). As a form of controlled environment agriculture, The VF system allows for exact control of environmental parameters regarding light, temperature, humidity and carbon dioxide (CO_2) levels to produce locally grown food (Avgoustaki and Xydis, 2019). Compared to traditional agriculture, VF can reduce water use by up to 95% through closed-loop irrigation, decrease land use by up to 90% (Avgoustaki and Xydis, 2020). It can also reduce the emission of CO_2 from food transportation and boost productivity in a precisely controlled environment (Ptak et al., 2024), thereby ensuring a more reliable, secure and sustainable food supply (Feng et al., 2024). With the support of systematic energy strategies, VF can not only serve as a sustainable food production unit to ensure local food security, but also become a low-carbon and high-energy-efficiency urban infrastructure (Li et al., 2025). Nevertheless, VF is also known for its high energy consumption (Rathor et al., 2024), which can consume 10-100 times more energy per unit yield.

To increase the production of VF, it is of importance to improve the rate of photosynthesis, a key indicator of plant growth (Caporn, 1989). CO_2 is an indispensable substance for photosynthesis and can obviously influence plant growth velocity in VF systems (Flexas et al., 2007; Melkonian et al., 1998). Although the atmospheric CO_2 concentration has surged due to fossil fuel utilization and various anthropogenic activities (Zhou et al., 2024), the current CO_2 level cannot make plant photosynthesis at the highest capacity, due to the unsaturated activity of Ribulose-1,5-bisphosphate carboxylase/oxygenase (RuBisCO), particularly in plants belonging to the 3-carbon (C3) biochemical type (Gamage et al., 2018), which typically has an optimal CO_2 concentration for growth around 1000–1500 ppm (Chen, 2010). Moreover, in high-density planting or enclosed environments like VF, CO_2 concentration can be further decline by plant consumption with photosynthesis, and insufficient CO_2 can inhibit plant growth (Zhang et al., 2014). However, it doesn't mean increasing CO_2 concentration is always preferred. When CO_2 concentration exceeds the optimal level for growth, it can trigger negative physiological effects, such as the decrease in stomatal conductance and respiration, ultimately limiting plant growth (Calvert and Slack, 1975; Peet and Willits, 1984). Therefore, to enhance crop production in VF, CO_2 enrichment must be carefully regulated to maintain concentrations within the optimal range. This has been well recognized by numerous studies, as summarized in Table 1.

In addition to supplementing CO_2, understanding its spatial distribution is crucial to optimize energy efficiency and plant growth to achieve efficient resource use in VF (Carbonnel et al., 2022; Kang et al., 2024; Lim and Kim, 2014). Computational Fluid Dynamics (CFD) is widely used to simulate CO_2 distribution, which can replace cumbersome field experiments. Representative examples are summarized in Table 2. For instance, Zhang et al. (2016) used CFD simulations to improve airflow distribution and airflow uniformity over the crop canopy surface an indoor plant factory system. Zhang et al. (2020) assessed the spatial distribution of CO_2 concentration in strawberry greenhouses and found that localised crop enrichment methods were effective in increasing the distribution of CO_2 around plants. However, they did not consider CO_2 uptake by plants in their models. Naranjani et al. (2022) simulated airflow and heat transfer in an indoor vertical aquaculture system to achieve a more homogeneous microclimate distribution and reduce energy consumption by optimizing the location of the inlets and outlets of airflow. Nonetheless, their model assumed a constant CO_2 consumption rate, neglecting the dynamic relationship between plant CO_2 uptake and fluctuating CO_2 concentrations. To improve this drawback, Boulard et al. (2017) and Zhang et al. (2022, 2023) introduced CO_2 diffusion resistance in their CFD models for modelling CO_2 distribution in a greenhouse. However, such a CO_2 diffusion resistance was simplified solely based on empirical equations from previous studies rather than incorporating the actual leaf microstructure, which may potentially compromise the accuracy of CO_2 uptake estimates. It can be concluded that due to the lack of a mechanistic representation of plant physiology, particularly the dynamic CO_2 uptake influenced by internal leaf anatomy existing CFD studies overlook the dynamic absorption of CO_2 by plants. The exclusion of leaf microstructure, a critical factor influencing gas exchange, limits the accuracy of CO_2 uptake predictions and reducing the reliability of model outcomes.

This study aims to develop a more reliable CFD model to optimize CO_2 enrichment strategies and resource utilization efficiency in VF systems. The core contributions include:

Table 1
Positive effects of CO_2 enrichment on plants.

Authors	Crop	Experimental factors	Enhanced performance
Högy and Fangmeier (2009)	Potato	CO_2 enrichment	Increasing production by 17%-36%
Thongbai et al. (2010)	Tomato	CO_2 enrichment	Increasing the photosynthetic rate increased an average of 2.1 times
Xin et al. (2015)	Cucumber, Tomato, Strawberry, Chili, Zucchini, Eggplant	CO_2 enrichment	Increasing yields by 30%-35% and the crop maturity accelerated by about 6.87 days on average
Ahmed et al. (2022)	Lettuce	CO_2 enrichment, light intensity and air velocity	Increased fresh and dry weights of lettuce plants by 36.2% and 20.1%, respectively
Holley et al. (2022)	Lettuce	CO_2 enrichment	Increasing fresh and dry weight by 28% and 26%

Table 2
CFD modelling studies.

CFD[a] model				Plant model		
Authors	Dimension	Purpose	Validation	Considered parameters	Validation	Limitations
Zhang et al. (2016)	3D[a]	Design of an improved air circulation system with porous jet air tubes in a plant factory system	Average errors on air temperature and air velocity: 8.9% and 7.5%.	the effect of plants on airflow	NA	Not including CO_2 uptake by plants
Boulard et al. (2017)	3D	Simulating climate parameters inside the modelled closed greenhouse, including temperature, water vapour and CO_2 distribution	Mean errors for air temperature, leaf temperature, and air humidity: 6.7%, 7.4%, and 5.9%.	Leaf area density, Crop height, temperature, air humidity, solar radiation intensity.	Average errors in CO_2 concentration and CO_2 uptake: about 7.8% and 9.8%.	Not considering the resistance encountered by CO_2 in the actual microstructure of the leaf.
Zhang et al. (2020)	3D	Comparing two CO_2 enrichment methods for strawberry greenhouses	The Root Mean Squared Percentage Error (RMSPE[a]) on CO_2 concentrations: 3.5%, 4.3%, and 3.9% at 14, 18 and 24°C, and 7.4% for localised enrichment.	the effect of plants on airflow	Empirical CO_2 distribution	Not including CO_2 consumption by crops
Naranjani et al. (2022)	3D	Simulating air flow, temperature, humidity, CO_2 distribution, and plant photosynthesis in indoor vertical farming systems with four trays for hydroponic lettuce growth	Average errors of the normalized average velocity and the local Nusselt number along the center line: 5.2% and 8.7%.	CO_2 consumption rate, O_2 production rate, H_2O transpiration rate	The tray near the middle height (tray 3) had the lowest CO_2 and highest H_2O concentrations due to less effective circulation.	Not considering the variation of plant CO_2 consumption rate with CO_2 concentration
Zhang et al. (2022)	3D	Simulating CO_2 diffusion in three commercial strawberry greenhouses with different geometrical characteristics mulated.	Average absolute errors on air temperature, relative humidity and CO_2 concentrations: 1.7°C, 7.2% and 50.6 μmol^{-1}	maximum carboxylation rate, CO_2 compensation point, CO_2 concentration, temperature, relative humidity	Root mean square error is 2.1 $\mu mol\ m^{-2} \cdot s^{-1}$.	Not considering the resistance encountered by CO_2 in the actual microstructure of the leaf. Assumed the mesophyll conductance to be infinite, mesophyll resistance simplified.
Zhang et al. (2023)	3D	Simulating local and global CO_2 enrichment in a strawberry greenhouse	Root mean squared errors on air temperature, relative humidity and CO_2 concentrations:1.3°C, 6.9% and 79.2 μmol^{-1}	CO_2 concentration, temperature, relative humidity, maximum carboxylation rate		

[a] CFD: Computational Fluid Dynamics; 3D: 3 Dimensions; RMSPE: Root Mean Squared Percentage Error.

- Integrating the microscopic structure of leaves with the physiological mechanism of CO_2 diffusion to a 3D CFD model.
- Evaluating the impacts of various key parameters, i.e. different mass flow rates and CO_2 supply concentrations, on CO_2 distribution and CO_2 consumption.
- Providing suggestions about the design and control of CO_2 supplementation strategies to reduce operational costs, and enhance the resource efficiency of VF systems.

2. Methodology

The structure of the model framework is illustrated in Fig. 1. To simulate the diffusion and distribution of CO_2 in the VF chamber, a CFD model is developed in ANSYS FLUENT 2021R1 to simulate the changes in CO_2 concentration. To simulate the CO_2 uptake process in plants, a plant model proposed by Ho et al. (2012) that incorporates leaf microstructure is constructed using COMSOL Multiphysics (version 6.0, COMSOL AB, Stockholm, Sweden).

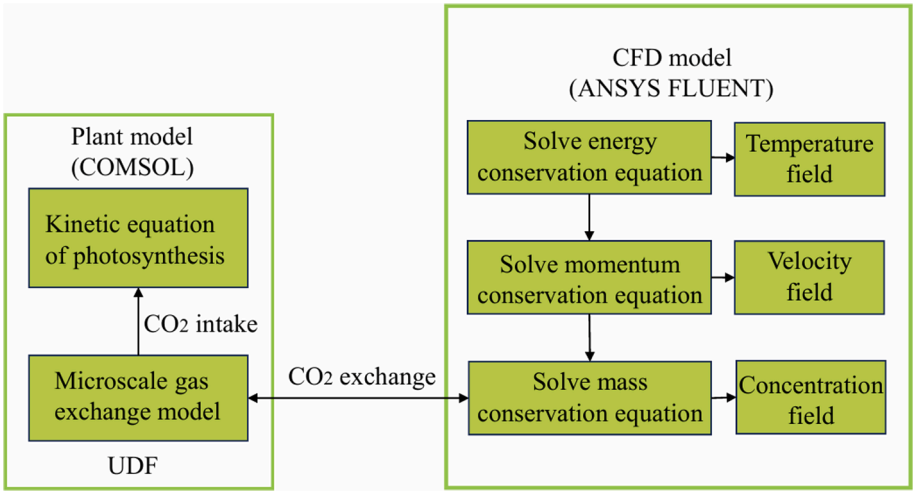


Fig. 1. Model structure. CFD: Computational Fluid Dynamics; UDF: User-Defined Functions.

2.1. CFD model

It is assumed that the flow inside the growth chamber is an incompressible Newtonian fluid. To simulate its flow, the mass, momentum and energy balances are described by Eqs. (1)–(3) below:

$$\frac{\partial \rho}{\partial t}+\frac{\partial}{\partial x_i}(\rho u_i)=0 \tag{1}$$

$$\frac{\partial}{\partial x_j}\left(\rho u_i u_j\right)=\frac{\partial}{\partial x_j}\left[-P+\mu\left(\frac{\partial u_i}{\partial x_j}+\frac{\partial u_j}{\partial x_i}\right)\right]+\rho g_i+S_m \tag{2}$$

$$\frac{\partial}{\partial x_j}\left(\rho u_j C_p T\right)=\frac{\partial}{\partial x_j}\left(\lambda\frac{\partial T}{\partial x_j}\right)+S_T \tag{3}$$

where $i, j = 1, 2, 3$, and x_j represents the direction in the 3D Cartesian coordinate system. In addition, ρ, u_j, μ, and T denote density, time-averaged velocity, effective dynamic viscosity, and the time-averaged temperature, respectively. In Eq. (2), ρg_i denotes the buoyancy influence within the momentum equation, λ is the thermal conductivity, C_p denotes specific heat capacity, S_m is the custom source term, and S_T is the heat sink or heat source. Since it is also assumed that the chamber is insulated, S_T remains zero across the entire computational domain. This study uses the standard k-ε turbulence model to simulate the airflow distribution in the growth chamber. Although it may have limited performance in strong swirling flows and complex near-wall recirculation zones, such a model has been widely employed for room-scale airflow mixing, greenhouse ventilation, and porous plant canopy simulations in controlled environment agriculture (Kang et al., 2024; Zhang et al., 2023), which have demonstrated good accuracy.

The fluid in the growth chamber is a mixture of water vapour, oxygen, CO_2 and nitrogen. In convective diffusion of a mixture, the mass fraction of the substance Y_i satisfies the conservation equation shown in Eq. (4):

$$\frac{\partial}{\partial t}(\rho Y_i)+\nabla\cdot(\rho\vec{v}Y_i)=-\nabla\vec{J}_i+R_i+S_i \tag{4}$$

where J_i represents the diffusive flux of substance i, R_i represents the net production rate of the chemical reaction, S_i represents the discrete phase and the additional production rate due to the source term, ρ denotes the density, kg m^{-3} and ν denotes diffusion velocity, $m{\cdot}s^{-1}$.

In turbulent flow, the mass diffusion flux of substance i is calculated by Eq. (5):

$$\vec{J}_i=\left(\rho D_{i,m}+\frac{\mu_t}{S}\right)\nabla Y_i \tag{5}$$

where $D_{i,m}$ represents the diffusion coefficient of the i-th substance in the mixture, $m{\cdot}s^{-1}$ and S denotes the Schmidt number of turbulence, which is 0.7 by default.

Due to the difficulty of modelling the geometry of real plants, the growing area is simplified to a porous medium with a parallel hexagonal shape, which was proposed by (Boulard and Wang, 2002). When the porous media model is used, the crop induced resistance related to the sink term (S_m) in the momentum equation is incorporated into the CFD model through the Darcy-Forchheimer equation (Eq. (6)):

$$S_m=-\left(\left(\frac{\mu}{K_p}\right)\cdot\nu+\left(\frac{C_F}{\sqrt{K_p}}\right)\cdot\rho\cdot\nu^2\right) \tag{6}$$

where μ, K_p, ν, C_F, and ρ denote aerodynamic viscosity, $kg{\cdot}m^{-1}{\cdot}s^{-1}$, permeability of porous medium, m^2, diffusion velocity, $m{\cdot}s^{-1}$, nonlinear momentum loss coefficient, and air density, $kg{\cdot}m^{-3}$, respectively. When simulating plants, the linear term can be ignored, because under typical air flow conditions in plant canopies, inertial resistance is much greater than viscous resistance (Boulard and Wang, 2002). So only the second part of Eq. (6) will be considered in this study. In addition, the momentum sink term is proportional to the leaf area density and the unit volume of the canopy can be expressed by Eq. (7) (Majdoubi et al., 2009):

$$S_m=-\rho{\cdot}LAD{\cdot}D{\cdot}\nu^2 \tag{7}$$

where, LAD denotes the leaf area density, representing the unilateral leaf area contained in a unit volume of the crop canopy (unit: $m^2{\cdot}m^{-3}$); and D denotes the drag coefficient, a dimensionless parameter representing the aerodynamic resistance of the plant canopy to airflow, which describes the obstruction effect of crop leaves on air flow and CO_2 convective transfer in the growth chamber.

2.2. Plant model

The plant model is used to simulate the dynamic changes in photosynthetic rate in varied atmospheric CO_2 concentrations to generate the relationship between photosynthetic rate and CO_2 concentration. Then such a relationship is correlated by a function, which is further embedded into the Fluent User-Defined Functions (UDF) module. To extend the CO_2 absorption rate from the 2D leaf model to the 3D planting area, leaf area density (LAD, measured in $m^2{\cdot}m^{-3}$) is introduced, which denotes the one-sided leaf area per unit volume. Then the CO_2 absorption rate across the 3D planting area is quantified by multiplying the photosynthetic rate obtained from the 2D leaf model by LAD and the volume of the 3D planting area.

In this paper, the Farquhar–von Caemmerer–Berry (FvCB) model is used to describe the total CO_2 fixation rate A_G in chloroplasts of C3 plants (Farquhar et al., 1980; Sharkey, 1985; Yin et al., 2004), as shown in Eq. (8):

$$A_G=\left(1-{}^{\Gamma^*}/_{C_c}\right)\min(w_c,w_j,w_p) \tag{8}$$

where, w_c denotes the Rubisco limiting rate of carboxylation, w_j is the RuBP regeneration or electron transfer limiting rate, w_p is the trisaccharide phosphate utilization (TPU) limiting rate, in which are expressed by Eqs. (9)–(11) below:

$$w_c=\frac{C_c\cdot V_{c,max}}{C_c+K_{m,C}\left(1+\frac{O_2}{K_{m,O_2}}\right)} \tag{9}$$

$$w_j=\frac{C_c\cdot J}{4C_c+8\Gamma^*} \tag{10}$$

$$w_p=\frac{3T_p}{\left(1-\frac{\Gamma^*}{C_c}\right)} \tag{11}$$

where C_c and O_2 represent CO_2 and O_2 concentrations within chloroplasts, J denotes the electron transfer rate, T_p denotes the chloroplasts export rate of the triose phosphate, and $K_{m,C}$, K_{m,O_2} and $V_{c,max}$ are constants, which are introduced by Bernacchi et al. (2001).Rubisco antisense transgenic tobacco was used as material and leaf gas exchange measurements were conducted at different temperatures and CO_2/O_2 concentrations. By fitting the Michaelis equation and Arrhenius temperature response equation, these standard values were determined, verifying that they were the standard parameters of the C3 photosynthesis model.

Potential electron transport flux in Eq. (10) is calculated as in Eq. (12)

$$J=\frac{sI_{inc}\Delta F}{F_m'} \tag{12}$$

where, s denotes the calibration factor, I_{inc} denotes the flux density of photons incident on the leaves, F_S is the steady-state fluorescence, and F_m' represents the peak fluorescence achieved during a fully saturating light pulse (Genty et al., 1989).

CO_2 exchange in leaf tissue can be described by the reaction-diffusion Eqs. (13) and (14):

$$\frac{\partial C}{\partial t} = \nabla \cdot D \nabla C - A_G^* + R_d^* + B \tag{13}$$

$$\frac{\partial C_{HCO_3^-}}{\partial t} = \nabla \cdot D_{HCO_3^-} \nabla C_{HCO_3^-} - B \tag{14}$$

where C and $C_{HCO_3^-}$ are the local CO_2 and HCO_3^- concentrations, D and $D_{HCO_3^-}$ represent the respective local diffusion coefficients, t is time, A_G^* is the overall volumetric photosynthesis rate of chloroplasts and A_G^* and R_d^* are calculated from A_G and R_d with the following Eqs. (15) and (16):

$$A_G^* = \frac{A_G}{d \cdot f_c} \tag{15}$$

$$R_d^* = \frac{R_d}{d \cdot f_m} \tag{16}$$

where d is the leaf's average thickness, f_c and f_m are the proportions of chloroplasts and cytoplasm, respectively, in the two-dimensional cross-section of the leaf.

B in Eqs. (13) and (14) denotes the net hydration rate for the conversion of CO_2 to HCO_3^-, as expressed by Eq. (17):

$$B = k_2 \frac{[H^+] C_{HCO_3^-,c}}{K} - k_1 C_c \tag{17}$$

where k_1 is the CO_2 hydration velocity constant, k_2 is the CO_2 dehydration velocity constant, and K is the acidity constant of carbonic acid.

CO_2 fluxes through cell membranes, chloroplasts and vesicle membranes are described by boundary conditions, as shown in Eq. (18):

$$\phi = -P_m \Delta C \tag{18}$$

where P_m is the membrane permeability.

The local CO_2 concentrations are assumed to maintain equilibrium at all times, as governed by Henry's law, ignoring the effect of temperature on the model.

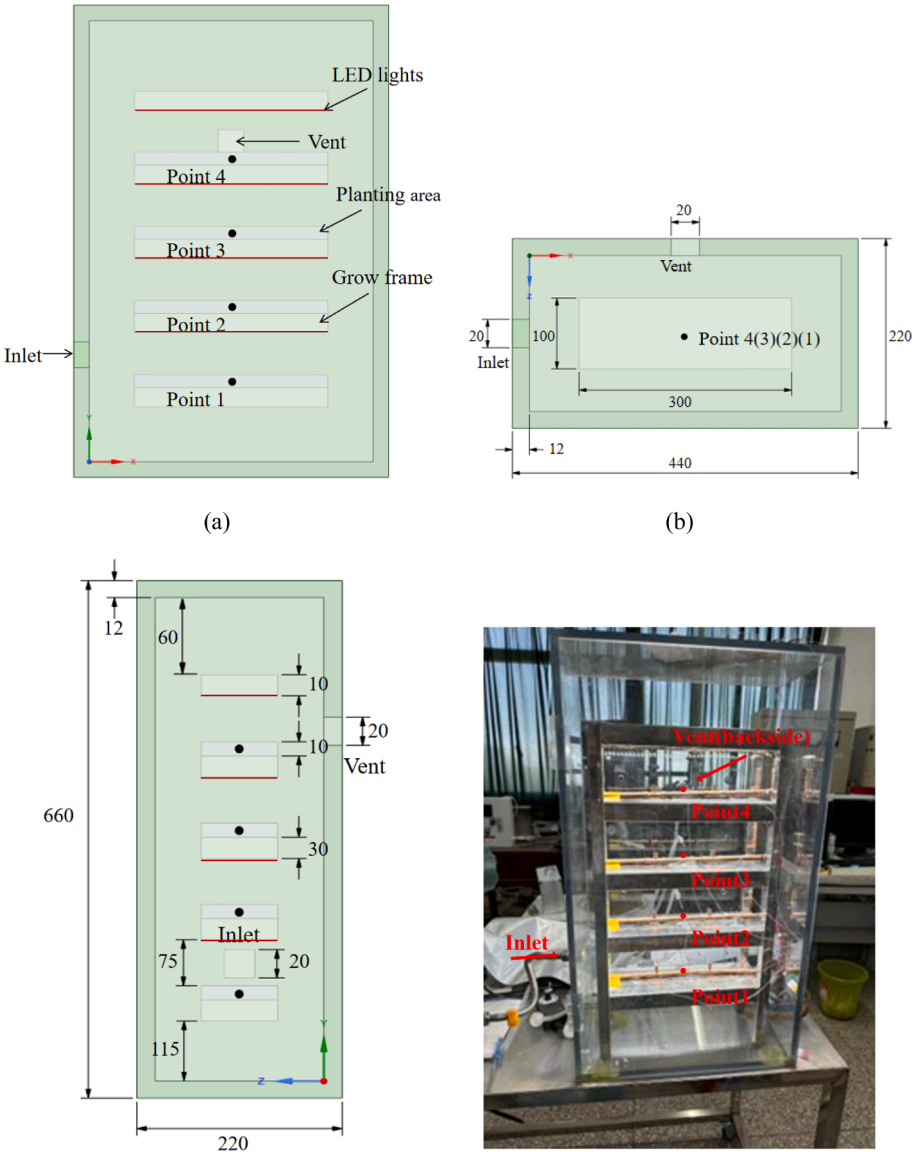


Fig. 2. Schematic diagram of the test chamber (in mm): (a) front view of the test chamber, (b) top view, (c) side view, and (d) photo of the test chamber.

2.3. Validation of the CFD model

2.3.1. Testing chamber description

To validate the CFD model, a test chamber, sketched in Fig. 2(a), which consists of LEDs, grow frames and planting areas, was built and experiments were conducted. The LEDs are distributed evenly on the bottom of the grow shelf area (red line). The dimensions of the chamber are shown in Fig. 2(b) and (c), with units in mm. The centers of the planting areas in each layer are designated as points 1 to 4 in Fig. 2. To save cost and time, the test was simplified that no real plant was placed in the chamber. In order to mimic CO_2 uptake by plants, an air pump was used to withdraw air from each layer at the center. The withdrawn air was collected into a bag to measure the CO_2 consumption. There is a vent in the chamber that is used to balance the inside pressure to be atmospheric pressure.

2.3.2. Measurement instruments

A gas flow meter (NRRS series, Nanjing Ruiji Automation Co., Ltd, ±1.5%, 0–65 $Nm^3 \cdot h^{-1}$) was used to control the velocity of CO_2 enriched air. The changes in CO_2 concentrations at the four measurement points were recorded using a CO_2 sensor (B1010-CO_2 series, Shenzhen WOSETE Technology Co., Ltd, ±3%, 0 to 50000 ppm). Finally, the CO_2 concentration in the collecting bag was measured and the amount of withdrawn CO_2 was calculated.

2.3.3. Test conditions

When the test started, CO_2-enriched air was injected into the chamber at a constant velocity flow. After 15 min, the injection was stopped, and the air pump started to withdraw air from the chamber until the CO_2 concentration dropped to 400 ppm. The rated power, and rotation speed of the air pump were 10 W, and 15000 $r \cdot min^{-1}$ respectively. The velocity of CO_2-enriched air was set to 0.3, 0.5, and 0.7 $m \cdot s^{-1}$, with an inlet air temperature of 300 K, and CO_2 concentration of 10000 ppm. The initial CO_2 concentration was set at 400 ppm, and the test conditions are summarized in Table 3.

2.3.4. Model verification and validation

According to the geometry of the test chamber, the mesh of the CFD model was created, and the boundary conditions and key inputs are listed in Table 4. In order to test the mesh independence, three grids were checked, which were created using an unstructured mesh with a mixture of tetrahedral, pyramid and hexahedral. By following other studies, e.g. Naranjani et al. (2022), Kibwika et al. (2023), and Gu and Goto (2024), the air inlet flow velocity was set to 0.5 $m \cdot s^{-1}$. Fig. 3 describes the variation of CO_2 concentration with grid numbers at four points. It was clear that when the grid number was over 680000, the change in CO_2 concentration was less than 0.3%. Therefore, 680000 was selected for the other numerical simulations in this work.

Fig. 4 and Table 5 present a comparison between the simulated and measured CO_2 concentrations under various inlet velocities. In general, the simulation results aligned well with the measurements, with all errors less than 5%, although some minor deviations could still be observed. In general, the larger the flow rate, the larger the error. The maximum error occurs at point 1, which is 4.83%.

Table 3
Test conditions.

Parameters	Values
Inlet Velocity	0.3, 0.5, and 0.7 $m \cdot s^{-1}$
LED[a] heat flux	300 $W \cdot m^{-2}$ (32W)
Wall temperature	300 K
CO_2-enriched air temperature	300 K
CO_2-enriched air concentration	10000 ppm
Initial room CO_2 concentration	400 ppm
Planting zone volume	0.3 m × 0.1 m × 0.01 m

[a] LED: Light-Emitting Diode.

Table 4
Boundary conditions and key inputs.

Parameters	Value
Aluminum Density	2719 $(kg \cdot m^{-3})$
Aluminum Specific heat	871 $(J \cdot kg^{-1} \cdot K^{-1})$
Aluminum Thermal conductivity	202.4 $(W \cdot m^{-1} \cdot K^{-1})$
CO_2-enriched air	Incompressible-ideal gas
CO_2-enriched air specific heat	Mixing-law
CO_2-enriched air thermal conductivity	0.024 $(W \cdot m^{-1} \cdot K^{-1})$
Wall density	900 $(kg \cdot m^{-3})$
Wall specific heat	2550 $(J \cdot kg^{-1} \cdot K^{-1})$
Wall thermal conductivity	0.29 $(W \cdot m^{-1} \cdot K^{-1})$
LAD[a] (Allison, 1964)	6.2 $m^2 \cdot m^{-3}$
D[a] (Zhang et al., 2022)	0.32
Volumetric flow rate of withdrawn air	38 $m^3 \cdot h^{-1}$

[a] LAD: leaf area density; D: drag coefficient.

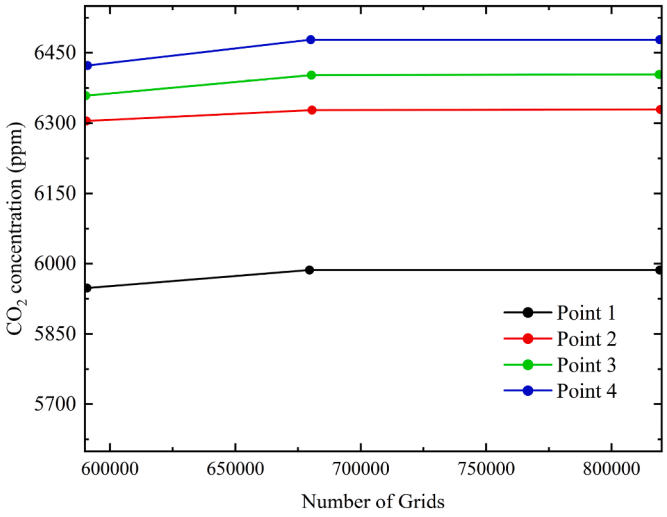


Fig. 3. CO_2 concentration at measurement points at equilibrium with different numbers of grids at a flow velocity of 0.5 $m \cdot s^{-1}$.

2.4. Validation of the plant models

Wheat was chosen as the plant studied in this work because of two reasons: (1) wheat was a typical C3 crop and itsphotosynthetic pathway can represent the absorption patterns of CO_2 in most leafy vegetables grown in vertical farms, such as lettuce and spinach (Wu et al., 2024), and (2) the data availability.

2.4.1. Geometric structure of wheat leaves

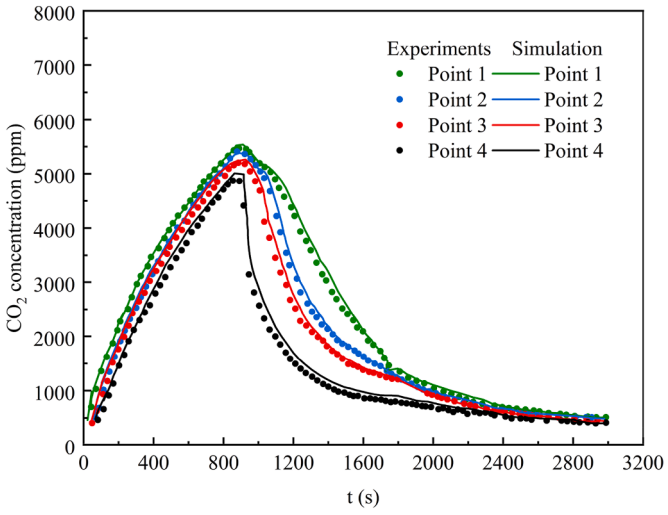
The 2D geometric structure of wheat leaves was constructed based on the optical microscope images of wheat leaves obtained from the literature (Hu et al., 2005). The images were digitized using Matlab R2021a (Fig. 5), with specific dimensions provided by Hu et al. (2005).

2.4.2. Assumptions and initial and boundary conditions

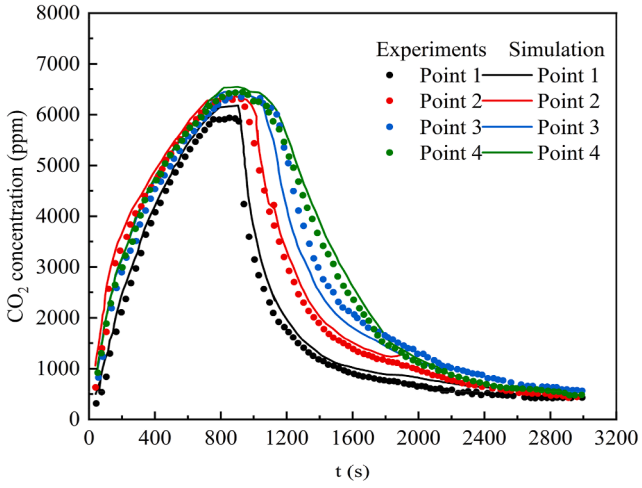
To examine the diffusion behavior of CO_2 within the leaf microstructure, Ho et al. (2012) established a microscale modeling framework for wheat leaves, which was subsequently validated using experimental data obtained by Yin et al. (2009). This model was replicated in this work. The required inputs and experimental conditions are detailed in Table 6 (Ho et al., 2012; Yin et al., 2009).

2.4.3. Model verification and validation

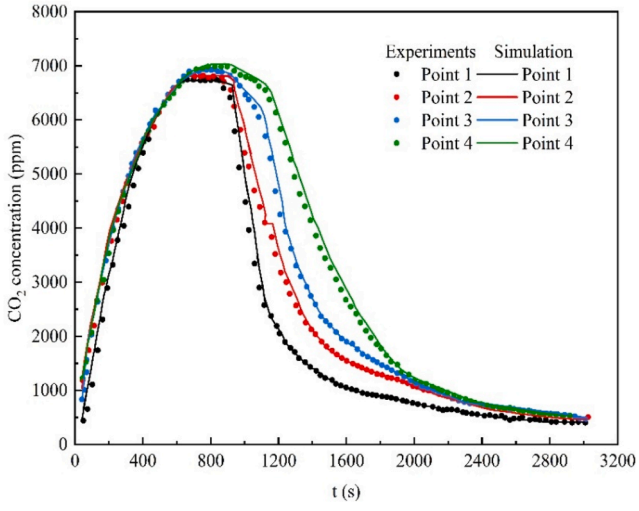
The plant model was verified and validated through comparisons with the simulated results from Ho et al. (2012) and the experimental data of Yin et al. (2009). Fig. 6 shows the simulation results of photosynthesis rate at a light intensity of 1000 $\mu mol \cdot m^{-2} \cdot s^{-1}$. The average relative errors



(a) Flow rate of 0.3 m·s^{-1}



(b) Flow rate of 0.5 m·s^{-1}



(c) Flow rate of 0.7 m·s^{-1}

Fig. 4. Dynamic changes in measured and simulated CO_2 concentration (ppm) at four points under different flow rates (0.3 m·s^{-1}, 0.5 m·s^{-1}, and 0.7 m·s^{-1}) over time (s).

Table 5
Average relative errors on CO_2 concentration under different air velocities.

Average error	flow rate of 0.3 m·s^{-1}	flow rate of 0.5 m·s^{-1}	flow rate of 0.7 m·s^{-1}
Point 1	2.75%	3.89%	3.95%
Point 2	2.53%	3.43%	3.51%
Point 3	2.42%	3.21%	3.23%
Point 4	2.39%	3.15%	3.17%

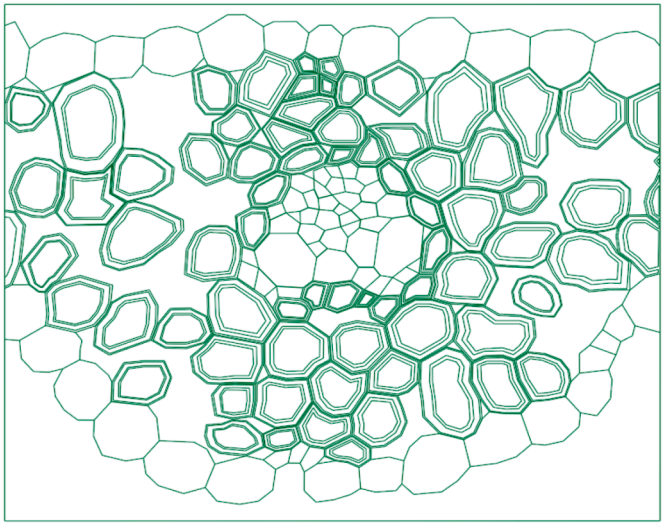


Fig. 5. Microscale geometry of the leaf.

Table 6
Specific values of physiological parameters used for plant modelling in this study (Ho et al., 2012; Yin et al., 2009).

Parameters	Symbol	Values
Diffusivity		
- Pore	$D_{CO_{2,g}}$	1.60×10^{-5} m^2·s^{-1}
- Cytosol and stroma	$D_{CO_{2,l}}$	1.67×10^{-9} m^2·s^{-1}
- Cell wall	D_w	3.437×10^{-7} m^2·s^{-1}
- Epidermis	D_{epi}	1.672×10^{-7} m^2·s^{-1}
Diffusion rate of HCO_3^- in the cytoplasm of leaf mesophyll cells	$D_{HCO_3^-,c}$	1.17×10^{-9} m^2·s^{-1}
Average thickness of the leaf	d	184 μm
Cell wall thickness	L_w	0.5 μm
Proportion of chloroplasts in the leaf	f_c	0.104
Proportion of cytoplasm in the leaf	f_m	0.169
Membrane permeability	P_m	3.5×10^{-3} m·s^{-1}
Henry's constant	H	0.83 (mol·m^{-3} liquid) (mol·m^{-3} gas)$^{-1}$
CO_2 hydration velocity constant	k_1	0.039 s^{-1}
	k_2	23 s^{-1}
Acidity constant of carbonic acid	K	2.5×10^{-4} mol·L^{-1}
Maximum rate of carboxylation limited by Rubisco activity	$V_{c,max}$	65.8 ± 0.8 μmol·m^{-2}·s^{-1}
Michaelis-Menten constant of Rubisco[a] for CO_2 and O_2	$K_{m,C}$	168 ± 17 μbar
	K_{m,O_2}	473 mbar
Electron transport conversion factor	s	0.38
CO_2 compensation point based on Cc[a] without Rd[a]	Γ^*	34 μbar
Day respiration	R_d	1.317 μmol·m^{-2}·s^{-1}
The output rate of chloroplast triose phosphate	T_p	12.9 ± 0.13 μmol·m^{-2}·s^{-1}
The leaf temperature	T_{leaf}	298 K
O_2 volume fraction	φ_{O2}	21%
N_2 volume fraction	φ_{N2}	78%

[a] Rubisco: Ribulose-1,5-bisphosphate carboxylase/oxygenase; Cc: mesophyll CO_2 concentration (μmol·mol^{-1}); Rd: day respiration (μmol CO_2 m^{-2}·s^{-1}).

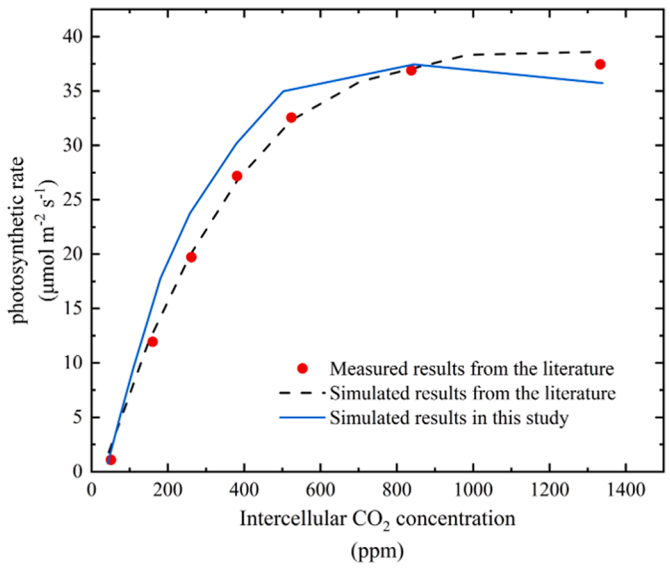


Fig. 6. Model validation on Photosynthetic rate of wheat leaves at the flowering stage under a light intensity of 1000 μmol·m^{2}·s^{-1} varying with intercellular CO_2 concentration.

are 3.8% and 7.6%, the maximum relative errors are 4.4% and 9.4%, and Root mean square errors (RMSE) are 0.8054 μmol·m^{-2}·s^{-1} and 2.319 μmol·m^{-2}·s^{-1} compared to the simulated results from Ho et al. (2012) and the experimental values of Yin et al. (2009).

2.5. System scaling up

To increase the practical relevance of the study, the geometry of the chamber was scaled up for further investigation. To achieve more efficient CO_2 distribution throughout the space, entrances were set on the top of the model. The improved growth chamber dimensions are shown in Table 7.

The chamber initial temperature was set to 298 K, the light intensity was 1000 μmol·m^{-2}·s^{-1}. The initial CO_2 concentration was set at 400 ppm, with oxygen concentration at 21%. The CO_2-enriched air inlet mass flow rate was maintained at 0.02 kg·s^{-1}, while the supplied CO_2 concentration was maintained at 2000 ppm. CO_2 injection started when the CO_2 concentration in the growth chamber dropped to 900 ppm, and stopped when it reached 1100 ppm. The ventilation system was activated during CO_2 injection and closed when the injection stops. The system adopted a mass flow inlet (0.02 kg·s^{-1}) and a pressure outlet boundary with a gauge pressure of 0 Pa (ambient atmospheric pressure, 101325 Pa). Assuming the flow was a completely turbulent mixture, in accordance with the standard k-ε turbulence model, all walls were subjected to slip free boundary conditions. During CO_2 dosing cycles, CO_2 loss was the total injection amount minus the amount of CO_2 absorbed.

2.6. Key performance indicator

To evaluate the performance of CO_2 distribution, the amount of CO_2 (E) absorbed by plants in the growing chamber due to photosynthesis is considered as a key performance indicator, which is estimated by Eq. (19):

$$E = \sum_{n=0}^{N} A \cdot LAD \cdot V \cdot \Delta t \tag{19}$$

where A denotes the photosynthetic rate, μmol·m^{-2}·s^{-1}, LAD denotes the leaf area density, m^{2}·m^{-3}, V denotes the volume of the growth domain, m^{3}, and t is the reaction time, s.

Table 7
Modified chamber dimensions.

Domain	Dimensions
Chamber	2.44 m × 1.34 m × 3.66 m
Planting area	1.5 m × 0.5 m × 0.1 m
Grow frame	1.5 m × 0.5 m × 0.15 m
Wall thickness	0.12 m
Inlet	2.2 m × 1.1 m
Outlet	0.2 m × 0.2 m

3. Results and discussion

In order to demonstrate the importance of implementing an accurate plant model in the CFD model (MC), a CFD model integrated with a simple plant model was also included for comparison, indicated as MS. The simple plant model did not include leaf microstructure, and assumed that the concentration of CO_2 in chloroplasts is equal to the concentration around the leaves, without involving the diffusion of CO_2 in the leaf microstructure.

3.1. Dynamic variation in CO_2 distribution

The CO_2 concentration profiles over time in the planting areas for the first three cycles are illustrated in Fig. 7. During the CO_2 injection phase, MC simulations showed that the average indoor CO_2 concentration stabilized at 1100 ppm after 238 s. After injection ceased, the CO_2 concentration in the planting area continued to rise due to a dynamic equilibrium between plant photosynthesis consumption and spatial diffusion, ultimately reaching a peak of 1057 ppm. This dynamic change reveals the lagged peak characteristic of CO_2 concentration in the planting area after injection cessation, which can be used to optimize CO_2 supplementation strategies. For example, when the concentration approaches 1100 ppm, injection can be stopped in advance to avoid excessive concentrations, while utilizing the peak plateau period to maintain efficient plant photosynthesis. Compared to MC, MS showed a faster CO_2 consumption rate, with a lower peak concentration of 1049 ppm. This difference highlights the importance of incorporating leaf microstructure into MC, which enables more accurate simulation of CO_2 concentration dynamics in closed environments by more realistically depicting CO_2 diffusion resistance. As a result, MC provides a more

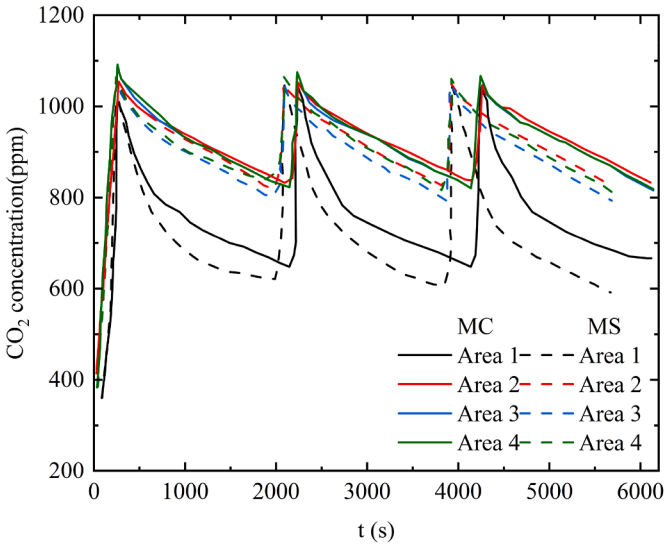


Fig. 7. Comparison of dynamic variations of CO_2 concentration (ppm) over time (s) in the four planting areas between the complex model (MC) and the simplified model (MS).

reliable theoretical basis for optimizing CO_2 management in vertical agriculture.

The distribution of CO_2 concentrations obtained by using MS and MC is compared in Fig. 8. The MC results showed the largest CO_2 concentration difference in planting area 1 (174 ppm) and the smallest in planting area 4 (16 ppm), reflecting the influence of distance of each planting area from the CO_2 inlet. Planting area 4, located adjacent to the top inlet, experienced shorter diffusion paths and more uniform CO_2 distribution. In contrast, planting area 1, the farthest from the inlet, exhibited greater diffusion resistance due to obstruction by planting racks, resulting in the greatest concentration gradient in this planting area.

Across all planting areas, the MS model consistently produced a larger concentration difference than the MC model, indicating a more heterogeneous CO_2 distribution. For example, the biggest difference was found in planting area 1, with a difference between the highest concentration and the lowest concentration of 174 ppm for the MC model compared to 259 ppm for the MS model. These results suggest that neglecting leaf microstructure in MS reduces the accuracy in capturing spatial CO_2 distribution, highlighting the importance of incorporating physiological detail in the MC model.

3.2. Dynamic variation in photosynthetic rate

The photosynthesis rate profiles over time for the first three cycles are depicted in Fig. 9. The MC simulation results showed that the photosynthetic rates of the four planting areas fluctuated with the change of CO_2 concentration in the planting areas. Based on the dynamic relationship between photosynthetic rates and CO_2 concentration in the MC simulation, the optimal CO_2 concentration range for plants can be estimated, and intermittent CO_2 supplementation can be used to maintain efficient photosynthesis in plants. The MC showed a relatively low photosynthetic rate, with a peak of 37.2 $\mu mol \cdot m^{-2} \cdot s^{-1}$, whereas the MS had a higher peak of 38.7 $\mu mol \cdot m^{-2} \cdot s^{-1}$. Furthermore, the MS demonstrated less variation in the photosynthetic rate throughout a single cycle. In planting area 1, the photosynthetic rate of the MS decreased by 1.6 $\mu mol \cdot m^{-2} \cdot s^{-1}$, while the MC showed a more significant decline of 5.8 $\mu mol \cdot m^{-2} \cdot s^{-1}$. This difference is primarily due to the faster CO_2 diffusion in MS than the MC, which leads to a more uniform CO_2 distribution and smoother photosynthetic response.

3.3. CO_2 consumption

Table 8 compares the number of injection cycles and CO_2 consumption obtained by using MS and MC over one day period. The MC simulation results showed a single cycle duration of 1986 s, with 43.5 cycles completed daily, corresponding to a daily CO_2 absorption rate of 124.9 g and a consumption rate of 139.3 g. These data provide an important basis for CO_2 injection strategies, such as reasonably setting injection intervals to avoid CO_2 waste caused by frequent injections, optimizing the control system to achieve precise timed injections to meet plant photosynthesis requirements while reducing unnecessary CO_2 consumption, and improving resource utilization efficiency.

The MS led to a shorter cycle length, which was 132 s shorter than the MC. As a result, for one day, the average number of cycles estimated by was 3.1 more than that estimated by the MC. Consequently, this increased cycle number further led to an increase in the amount of absorbed CO_2. The absorbed CO_2 calculated by using the MS was 10.1 g more than that calculated by using the MC, which means 8.1% more. In addition, some CO_2 can also be lost due to the ventilation. The consumed CO_2 obtained by using the MS was 8.5% more than that obtained by using the MC. The difference clearly highlighted the necessity to use the MC, which can take into account plant microstructural impediments to CO_2 diffusion, when studying the performance of CO_2 enrichment. This finding provides not only insights regarding the optimization of system design on CO_2 distribution for VFs, but also guideline regarding the

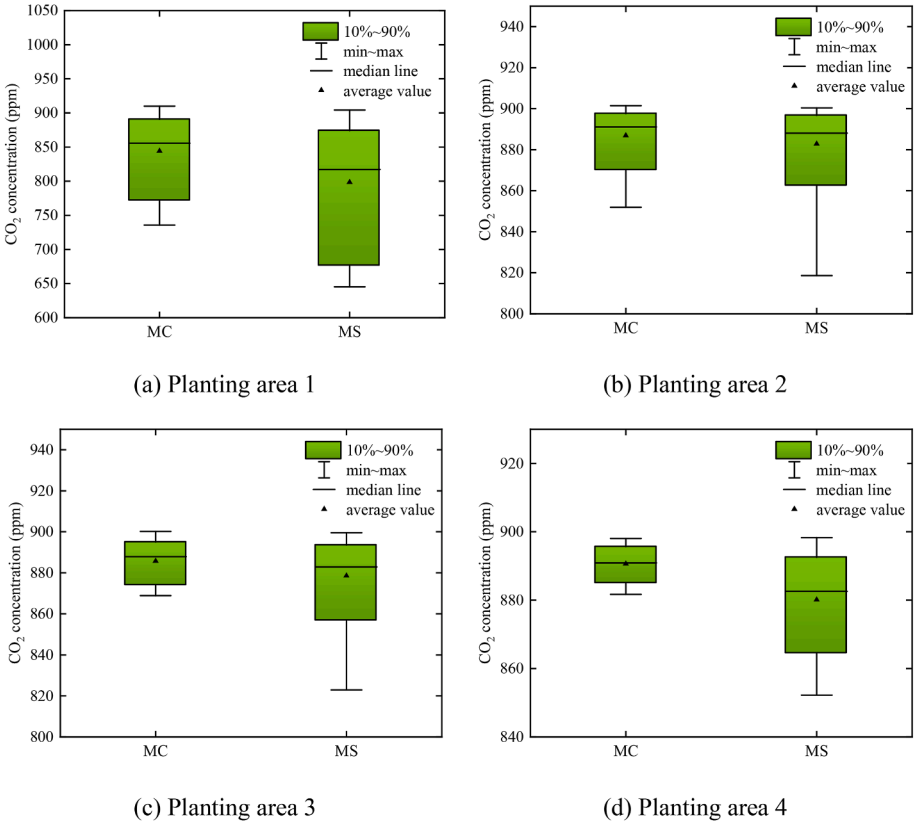


Fig. 8. Comparison of CO_2 concentration distributions in the four planting areas between the complex model (MC) and the simplified model (MS).

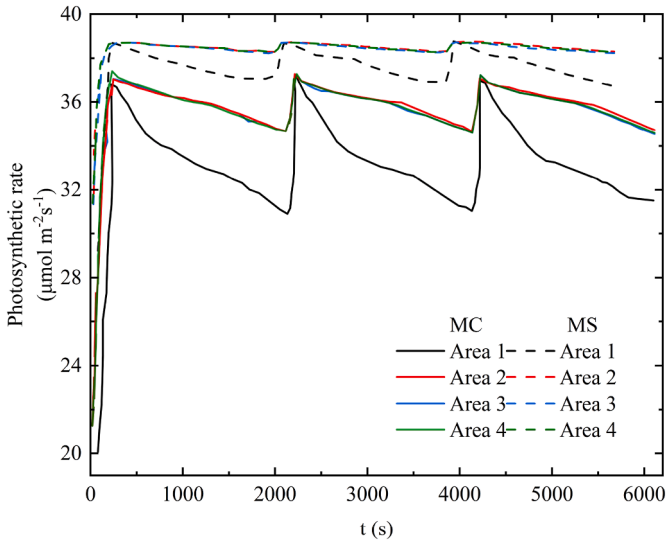


Fig. 9. Variation of photosynthetic rates (μmol·m^{-2}·s^{-1}) over time (s) in the four planting areas: a comparison between the complex model (MC) and the simplified model (MS).

development of control strategy and dynamic operation optimization, enabling more efficient resource utilization and higher crop yields.

3.4. Sensitivity analysis

The performance of CO_2 distribution can be clearly influenced by some key parameters, such as the injected air mass flow rate and the supply CO_2 concentrations. To quantify their impacts, sensitivity studies were conducted by using the developed model, as shown in Table 9.

The variation of daily CO_2 mass by plants with inlet air mass flow rates was shown in Fig. 10, which decreased with the increase of inlet mass flow rate. It implies that at low mass flow rates favor the plants. This is mainly due to uniformity of CO_2 distribution in the chamber. because there was only one injection point, when the CO_2 mass flow rate was higher, the CO_2 concentration on the layer closer to the inlet increased much faster than on other layers. As a result, it can result in a much less uniform CO_2 distribution. Since the injection was controlled according to the average CO_2 concentration in the chamber, such higher nonuniformity would lead to a shorter injection operation. This can be observed from the injected CO_2 mass in Fig. 10 therefore, the absorbed CO_2 declined.

Fig. 11 showed the variation of daily CO_2 absorption amount with supply CO_2 concentrations. In general, with the increase of the concentration, the absorption first rised and then declined, with a peak happening at the concentration of 2000 ppm. This is also due to the nonuniformity of CO_2 distribution in the chamber. According to the injected CO_2 amount shown in Fig. 11, when the supply CO_2 concentration was 2000 ppm, the injected CO_2 also reached the peak, which, hence, led to the peak of CO_2 absorption.

Table 8
Comparison between two models on the operation of CO_2 injection.

	Complex plant model (MC)	Simplified plant model (MS)	Difference
Cycle duration (s)	1986	1854	-6.6%
Cycle number per day	43.5	46.6	7.1%
Daily Absorption (g)	124.9	135.0	8.1%
Daily consumption of CO_2 (g)	139.3	151.0	8.5%

Table 9
Sensitivity analysis parameters.

Influence factors	Case 1	Case 2	Case 3
Inlet air mass flow rate (kg·s^{-1})	0.015	0.02	0.025
CO_2 supply concentration (ppm)	1800	2000	2200

3.5. Limitations and future work

This study proposed to integrate leaf microstructure into CFD simulations to capture the dynamic interaction between CO_2 diffusion and photosynthesis near plants, addressing a key limitation in previous studies that either relied on empirical resistance models or ignored diffusion within leaves. However, several simplifications were included, which show some limitations. The impacts of transpiration, light intensity, nutrient supply, temperature and humidity on plant photosynthetic were not considered. Transpiration is a core physiological process coupled with leaf gas exchange, and its neglection can affect the simulation on VF microclimate and CO_2 transport. A constant light intensity (1000 μmol·m^{-2}·s^{-1}) was also used in this work, ignoring the spatio-temporal variation of light in actual VF and its regulatory effect on photosynthesis. Moreover, it was also assumed that nutrient supply, temperature, and humidity didn't change, which may not be true. To further improve the model accuracy, such factors are suggested to be taken into account in the future work. In addition, plant growth stages were assumed to be static, neglecting dynamic growth changes limiting the model accuracy about predicting CO_2 consumption throughout the growth cycle, which should also be improved in the future study.

Even though the standard k-ε turbulence model has been validated and shows high computational efficiency to simulate turbulence, considering its limited accuracy for porous crop canopies, it is also suggested in the future work that other turbulence models should be employed to improve simulation accuracy, for example, the RNG k-ε turbulence model, which has a wider applicability and higher precision for complex flows.

The current CO_2 injection is not optimized in the studied system, such as the inlet geometry, air velocity, and the distribution system of CO_2. Further investigation on these system design parameters is recommended.

While wheat was used as a model crop due to data availability in this study, it is not typically cultivated in VF systems. To further validate the model's applicability, future studies should acquire key microstructural parameters for crops more commonly grown in VFs, such as lettuce, basil and other vegetable crops.

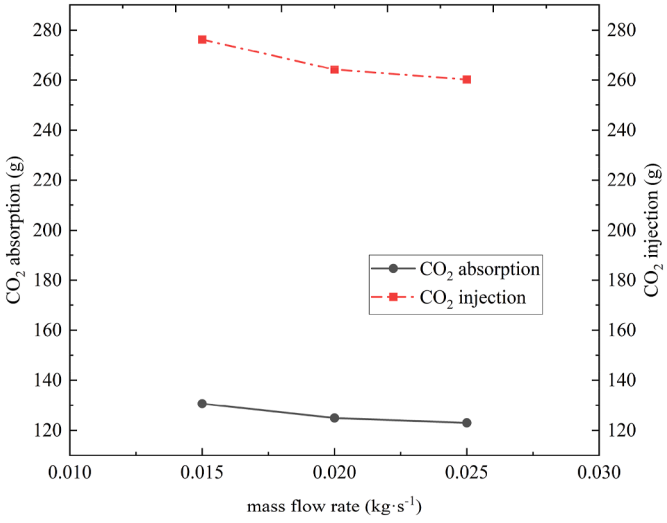


Fig. 10. Variation of daily CO_2 mass by plants under different inlet air mass flow rates.

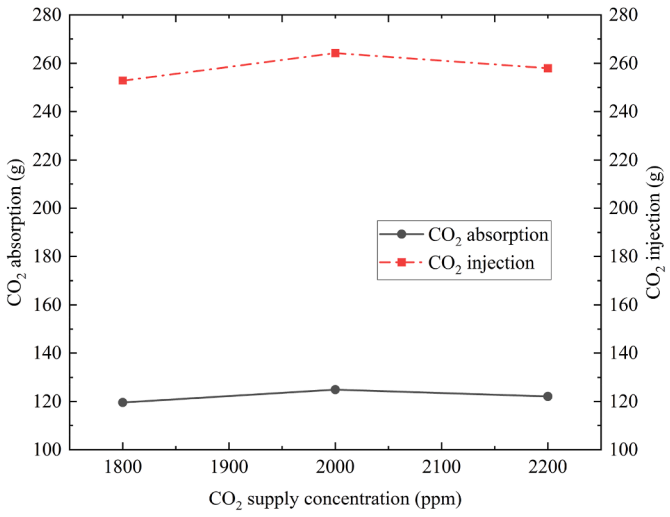


Fig. 11. Variation of daily CO_2 absorbed by plants under different CO_2 supply concentrations.

4. Conclusions

This study developed and validated a computational fluid dynamics (CFD) for Vertical farming (VF) to investigate CO_2 intake and distribution. To demonstrate its advantages, the developed complex model (incorporating the leaf microstructure, MC) was compared with a simplified model (ignoring the leaf microstructure, MS), from perspectives of CO_2 distribution, photosynthetic rate and total CO_2 consumption.

It is found that periodic injection of CO_2 can maintain CO_2 concentrations in the planting area within the optimal range, ensuring efficient photosynthetic rates for plants and providing a basis for optimizing CO_2 supplementation strategies. Additionally, spatial distribution of CO_2 concentration is gradient-related to inlet, which can guide the optimization of CO_2 supply. Based on the daily CO_2 absorption, consumption, and cycle duration, the injection interval and control frequency can be optimized to reduce waste of CO_2 and improve CO_2 utilization efficiency.

Compared with MS, incorporating leaf microstructure in MC can provide a more accurate representation of CO_2 dynamics in the studied VF. The MC also showed lower photosynthetic rate values and larger cyclical variations compared to the MS. In addition, for the daily CO_2 uptake, the MS showed an increase of 8.1% compared to the MC; and for the daily CO_2 consumption, the MS showed an increase of 8.5% compared to the MC, demonstrating that conventional approaches overestimate system efficiency due to unaccounted diffusion resistance.

CO_2 mass flow rate and supply concentration are key factors that can affect the performance of CO_2 enrichment. According to sensitivity analysis using MC, the CO_2 absorption declines with the increase of mass flow rate and there exists an optimal supply concentration, which was 2000 ppm for the studied chamber.

This study improves the understanding of the gas exchange process and provides a more accurate simulation model of CO_2 dynamics. The findings have practical implications for optimizing CO_2 enrichment strategies in controlled environments, such as VF, where precise CO_2 management is important for enhancing plant growth and improving resource use efficiency.

Statement

No generative AI or AI-assisted technologies were used during the preparation of this work.

CRediT authorship contribution statement

Shengchun Liu: Formal analysis, Investigation, Resources, Supervision, Writing – original draft. **Chenxing Wang:** Software, Validation, Visualization, Writing – original draft. **Lanfang Hu:** Data curation, Software, Validation, Visualization, Writing – original draft. **Luna Guo:** Data curation, Formal analysis, Resources, Supervision, Writing – review & editing. **Xiaolin Wang:** Formal analysis, Investigation, Writing – review & editing. **Anders Avelin:** Funding acquisition, Investigation, Resources, Supervision, Writing – review & editing. **Hailong Li:** Conceptualization, Formal analysis, Funding acquisition, Investigation, Project administration, Resources, Supervision, Writing – review & editing.

Declaration of competing interest

The authors declare that they have no known competing financial interests or personal relationships that could have appeared to influence the work reported in this paper.

Acknowledgements

This work was supported by the Knowledge foundation (KKS) (Sweden) under project Carbon2Food - Boosting sustainable vertical farming by CO_2 fertilization from air carbon capture (No. 20220040).

References

Ahmed, H.A., Tong, Y., Li, L., Sahari, S.Q., Almogahed, A.M., Cheng, R., 2022. Integrative effects of CO_2 concentration, illumination intensity and air speed on the growth, gas exchange and light use efficiency of lettuce plants grown under artificial lighting. Horticulturae 8 (3), 270. https://doi.org/10.3390/horticulturae8030270.

Allison, J.C.S., 1964. A comparison between maize and wheat in respect of leaf area after flowering and grain growth. J. Agric. Sci. 63 (1), 1–4. https://doi.org/10.1017/S0021859600014994.

Avgoustaki, D.D., Xydis, G., 2019. Plant factories in the water-food-energy Nexus era: a systematic bibliographic review. Food Secur. 12, 253–268. https://doi.org/10.1007/s12571-019-01003-z.

Avgoustaki, D.D., Xydis, G., 2020. Chapter one—how energy innovation in indoor vertical farming can improve food security, sustainability, and food safety?. In: Cohen, M.J. (Ed.), Advances in Food Security and Sustainability, vol. 5. Elsevier, pp. 1–51. https://doi.org/10.1016/bs.af2s.2020.08.002.

Bernacchi, C.J., Singsaas, E.L., Pimentel, C., Portis, Jr, A.R., Long, S.P., 2001. Improved temperature response functions for models of Rubisco-limited photosynthesis. Plant Cell Environ. 24, 253–259. https://doi.org/10.1111/j.1365-3040.2001.00668.x.

Boulard, T., Roy, J.-C., Pouillard, J.-B., Fatnassi, H., Grisey, A., 2017. Modelling of micrometeorology, canopy transpiration and photosynthesis in a closed greenhouse using computational fluid dynamics. Biosyst. Eng. 158, 110–133. https://doi.org/10.1016/j.biosystemseng.2017.04.001.

Boulard, T., Wang, S., 2002. Experimental and numerical studies on the heterogeneity of crop transpiration in a plastic tunnel. Comput. Electron. Agric. 34 (1–3), 173–190. https://doi.org/10.1016/S0168-1699(01)00186-7.

Calvert, A., Slack, G., 1975. Effects of carbon dioxide enrichment on growth, development and yield of glasshouse tomatoes. I. Responses to controlled concentrations. J. Hortic. Sci. 50 (1), 61–71. https://doi.org/10.1080/00221589.1975.11514604.

Caporn, S.J.M., 1989. The effects of oxides of nitrogen and carbon dioxide enrichment on photosynthesis and growth of lettuce (*Lactuca sativa* L.). New Phytol. 111 (3), 473–481. https://doi.org/10.1111/j.1469-8137.1989.tb00710.x.

Carbonnel, M. de, Stormonth-Darling, J.M., Liu, W., Kuziak, D., Jones, M.A., 2022. Realising the environmental potential of vertical farming systems through advances in plant photobiology. Biology 11 (6), 922. https://doi.org/10.3390/biology11060922.

Chen, L., 2010. Greenhouse environmental monitoring system with IPSO – BPNN computer measurement & control. Comput. Meas. Control 18 (3), 601–604+610. https://doi.org/10.16526/j.cnki.11-4762/tp.2010.03.063.

Dsouza, A., Newman, L., Graham, T., Fraser, E.D.G., 2023. Exploring the landscape of controlled environment agriculture research: a systematic scoping review of trends and topics. Agric. Syst. 209, 103673. https://doi.org/10.1016/j.agsy.2023.103673.

Farquhar, G.D., von Caemmerer, S., Berry, J.A., 1980. A biochemical model of photosynthetic CO_2 assimilation in leaves of C3 species. Planta 149 (1), 78–90. https://doi.org/10.1007/BF00386231.

Feng, Y., Gao, G., Wang, P., Zhang, Z., 2024. Integrating stakeholder value network with strategic issue management for multi-stakeholder needs and requirements analysis of vertical farming systems. Agric. Syst. 221, 104133. https://doi.org/10.1016/j.agsy.2024.104133.

Flexas, J., Diaz-Espejo, A., Galmés, J., Kaldenhoff, R., Medrano, H., Ribas-Carbo, M., 2007. Rapid variations of mesophyll conductance in response to changes in CO_2 concentration around leaves. Plant Cell Environ. 30 (10), 1284–1298. https://doi.org/10.1111/j.1365-3040.2007.01700.x.

Gamage, D., Thompson, M., Sutherland, M., Hirotsu, N., Makino, A., Seneweera, S., 2018. New insights into the cellular mechanisms of plant growth at elevated atmospheric carbon dioxide concentrations. Plant Cell Environ. 41 (6), 1233–1246. https://doi.org/10.1111/pce.13206.

Genty, B., Briantais, J.-M., Baker, N.R., 1989. The relationship between the quantum yield of photosynthetic electron transport and quenching of chlorophyll fluorescence. Biochim. Biophys. Acta Gen. Subj. 990 (1), 87–92. https://doi.org/10.1016/S0304-4165(89)80016-9.

Gu, X., Goto, E., 2024. Computational fluid dynamics model with realistic plant structures to study airflow in and around a plant canopy on a cultivation shelf in a plant factory with artificial light. Agriculture 14 (7), 1199. https://doi.org/10.3390/agriculture14071199.

Högy, P., Fangmeier, A., 2009. Atmospheric CO_2 enrichment affects potatoes: 1. Aboveground biomass production and tuber yield. Eur. J. Agron. 30 (2), 78–84. https://doi.org/10.1016/j.eja.2008.07.007.

Ho, Q.T., Verboven, P., Yin, X., Struik, P.C., Nicolaï, B.M., 2012. A microscale model for combined CO_2 diffusion and photosynthesis in leaves. PLoS One 7 (11), e48376. https://doi.org/10.1371/journal.pone.0048376.

Holley, J., Mattson, N., Ashenafi, E., Nyman, M., 2022. The impact of CO_2 enrichment on biomass, carotenoids, Xanthophyll, and mineral content of lettuce (Lactuca sativa L.). Horticulturae 8 (9), 820. https://doi.org/10.3390/horticulturae8090820.

Hu, Y., Fromm, J., Schmidhalter, U., 2005. Effect of salinity on tissue architecture in expanding wheat leaves. Planta 220 (6), 838–848. https://doi.org/10.1007/s00425-004-1401-8.

Kang, L., Zhang, Y., Kacira, M., Van Hooff, T., 2024. CFD simulation of air distributions in a small multi-layer vertical farm: impact of computational and physical parameters. Biosyst. Eng. 243, 148–174. https://doi.org/10.1016/j.biosystemseng.2024.05.004.

Kibwika, A.K., Seo, H.J., Seo, I.H., 2023. CFD model verification and aerodynamic analysis in large-scaled venlo greenhouse for tomato cultivation. AgriEngineering 5 (3), 1395–1414. https://doi.org/10.3390/agriengineering5030087.

Li, P., Dong, Y., Hamacher, T., 2025. Toward sustainable urban development: an integrated energy–economic–carbon optimization framework for vertical farming buildings. Energy Proc. 58. https://doi.org/10.46855/energy-proceedings-11882.

Lim, T.-G., Kim, Y.H., 2014. Analysis of airflow pattern in plant factory with different inlet and outlet locations using computational fluid dynamics. J. Biosys. Eng. 39 (4), 310–317. https://doi.org/10.5307/JBE.2014.39.4.310.

Majdoubi, H., Boulard, T., Fatnassi, H., Bouirden, L., 2009. Airflow and microclimate patterns in a one-hectare Canary type greenhouse: an experimental and CFD assisted study. Agric. For. Meteorol. 149 (6), 1050–1062. https://doi.org/10.1016/j.agrformet.2009.01.002.

Melkonian, J., Riha, S.J., Wilks, D.S., 1998. Simulation of elevated CO_2 effects on daily net canopy carbon assimilation and crop yield. Agric. Syst. 58 (1), 87–106. https://doi.org/10.1016/S0308-521X(98)00051-1.

Naranjani, B., Najafianashrafi, Z., Pascual, C., Agulto, I., Chuang, P.-Y.A., 2022. Computational analysis of the environment in an indoor vertical farming system. Int. J. Heat Mass Tran. 186, 122460. https://doi.org/10.1016/j.ijheatmasstransfer.2021.122460.

Peet, M.M., Willits, D.H., 1984. CO_2 enrichment of greenhouse tomatoes using a closed-loop heat storage: effects of cultivar and nitrogen. Sci. Hortic. 24 (1), 21–32. https://doi.org/10.1016/0304-4238(84)90004-9.

Ptak, M., Wasieńko, S., Makuła, P., 2024. A new approach to vertical plant cultivation maximises crop efficiency. Sustainability 16 (16), 7189. https://doi.org/10.3390/su16167189.

Rathor, A.S., Choudhury, S., Sharma, A., Nautiyal, P., Shah, G., 2024. Empowering vertical farming through IoT and AI-Driven technologies: a comprehensive review. Heliyon 10 (15), e34998. https://doi.org/10.1016/j.heliyon.2024.e34998.

Sharkey, T.D., 1985. Photosynthesis in intact leaves of C3 plants: physics, physiology and rate limitations. Bot. Rev. 51 (1), 53–105. https://doi.org/10.1007/BF02861058.

Thongbai, P., Kozai, T., Ohyama, K., 2010. CO_2 and air circulation effects on photosynthesis and transpiration of tomato seedlings. Sci. Hortic. 126 (3), 338–344. https://doi.org/10.1016/j.scienta.2010.07.018.

Vasavi, S., Anandaraja, N., Murugan, P.P., Latha, M.R., Pangayar Selvi, R., 2025. Challenges and strategies of resource poor farmers in adoption of innovative farming technologies: a comprehensive review. Agric. Syst. 227, 104355. https://doi.org/10.1016/j.agsy.2025.104355.

Wu, Z., Maga, D., Aryan, V., Reimann, A., Safarpour, T., Schillberg, S., 2024. A life cycle assessment of protein production from wheatgrass: optimization potential of a novel vertical farming system. Sustain. Prod. Consum. 51, 105–117. https://doi.org/10.1016/j.spc.2024.08.031.

Xin, M., Shuang, L., Yue, L., Qinzhu, G., 2015. Effectiveness of gaseous CO_2 fertilizer application in China's greenhouses between 1982 and 2010. J. CO2 Util. 11, 63–66. https://doi.org/10.1016/j.jcou.2015.01.005.

Yin, X., Struik, P.C., Romero, P., Harbinson, J., Evers, J.B., Van Der Putten, P.E.L., Vos, J., 2009. Using combined measurements of gas exchange and chlorophyll fluorescence to estimate parameters of a biochemical C $_3$ photosynthesis model: a critical appraisal and a new integrated approach applied to leaves in a wheat (*Triticum aestivum*) canopy. Plant Cell Environ. 32 (5), 448–464. https://doi.org/10.1111/j.1365-3040.2009.01934.x.

Yin, X., Van Oijen, M., Schapendonk, A.H.C.M., 2004. Extension of a biochemical model for the generalized stoichiometry of electron transport limited C $_3$ photosynthesis. Plant Cell Environ. 27 (10), 1211–1222. https://doi.org/10.1111/j.1365-3040.2004.01224.x.

Zhang, Y., Kacira, M., An, L., 2016. A CFD study on improving air flow uniformity in indoor plant factory system. Biosyst. Eng. 147, 193–205. https://doi.org/10.1016/j.biosystemseng.2016.04.012.

Zhang, Y., Yasutake, D., Hidaka, K., Kimura, K., Okayasu, T., Kitano, M., Hirota, T., 2023. Eco-friendly strategy for CO_2 enrichment performance in commercial greenhouses based on the CO_2 spatial distribution and photosynthesis. Sci. Rep. 13 (1), 17277. https://doi.org/10.1038/s41598-023-44200-9.

Zhang, Y., Yasutake, D., Hidaka, K., Kitano, M., Okayasu, T., 2020. CFD analysis for evaluating and optimizing spatial distribution of CO_2 concentration in a strawberry greenhouse under different CO_2 enrichment methods. Comput. Electron. Agric. 179, 105811. https://doi.org/10.1016/j.compag.2020.105811.

Zhang, Y., Yasutake, D., Hidaka, K., Okayasu, T., Kitano, M., Hirota, T., 2022. Crop-localised CO_2 enrichment improves the microclimate, photosynthetic distribution and energy utilisation efficiency in a greenhouse. J. Clean. Prod. 371, 133465. https://doi.org/10.1016/j.jclepro.2022.133465.

Zhang, Z., Liu, L., Zhang, M., Zhang, Y., Wang, Q., 2014. Effect of carbon dioxide enrichment on health-promoting compounds and organoleptic properties of tomato fruits grown in greenhouse. Food Chem. 153, 157–163. https://doi.org/10.1016/j.foodchem.2013.12.052.

Zhou, S., Li, L., Ji, L., Dai, B., Wang, Z., Benhelal, E., et al., 2024. Progress in recyclable chemicals for sustainable ex-situ CO_2 mineralisation. Green Energy and Res. 2 (3), 100087. https://doi.org/10.1016/j.gerr.2024.100087.